Journal of Photochemistry and Photobiology A: Chemistry 219 (2011) 10–15

Contents lists available at ScienceDirect

Journal of Photochemistry and Photobiology A: Chemistry

journal homepage: www.elsevier.com/locate/jphotochem

The characterisation of aerosol assisted CVD conducting, photocatalytic indium doped zinc oxide films

M.G. Nolan[a,*], J.A. Hamilton[a], S. O'Brien[a], G. Bruno[c], L. Pereira[d], E. Fortunato[d], R. Martins[d], I.M. Povey[a], M.E. Pemble[b]

[a] Advanced Materials and Surfaces Group, Tyndall National Institute, University College Cork, Lee Maltings, Ireland
[b] Tyndall National Institute, Department of Chemistry, University College Cork, Ireland
[c] Informatica e Sistemistica Università della Calabria Via P. Bucci, Arcavacata di Rende (CS), 41C I-87036, Italy
[d] Materials Science Department, CENIMAT/I3N and CEMOP/UNINOVA, FCT-UNL, Campus de Caparica, 2829-516 Caparica, Portugal

ARTICLE INFO

Article history:
Received 18 October 2010
Received in revised form 7 January 2011
Accepted 18 January 2011
Available online 26 January 2011

Keywords:
Zinc oxide
Doping
Photocatalysis

ABSTRACT

Indium doped, and undoped, zinc oxide films were deposited using aerosol assisted chemical vapour deposition (AACVD) at atmospheric pressure on glass substrates. Electrical measurements (*I–V*) showed a reduction in resistivity following the addition of indium, and XRD analysis revealed an associated switch to *c*-axis preferred crystal orientation. The ability of the films to oxidise organic material on their surface was analysed using stearic acid as the model contaminant under ultra-violet (UV, 365 nm) irradiation. The In-doped films displayed a greater rate of organic decomposition, which we attribute to the formation of a platelet surface structure having a larger surface area than the undoped films, on which the UV generated electrons and holes may react to form active photocatalytic species. In addition we suggest that the switch to *c*-axis crystal orientation may reduce the electron–hole pair recombination rate at the grain boundaries, due to an improvement in crystallinity and related reduction in carrier scattering losses, leading to an increase in photocatalytic organic decomposition rate.

1. Introduction

Previously reported applications of indium doped zinc oxide (In-ZnO) films include gas sensors [1], transparent anodes for organic light emitting diodes (OLEDs) [2], ohmic contacts in GaN LEDs [3], transparent electrodes in solar cells [4] and as channels in thin film transistors [5]. To date the authors are aware of only one investigation into the UV induced photocatalytic properties of In-ZnO films. Yanning et al. [6] studied the antibacterial properties of In-ZnO under ultra-violet irradiation, and saw an improved photocatalytic response following the addition of indium. However a number of groups have reported UV activated photocatalytic properties for elemental doped ZnO, where the dopant elements include silver [7–10], lanthanum [11–13], aluminium [14], palladium [15], and magnesium [16]. Doping to shift the absorbance band of ZnO into the visible portion of the solar spectrum has been reported through the addition of nitrogen [17–19], copper [20], tantalum [21], chromium [22], manganese [23], sulphur [24], carbon [24], co-doping with lanthanum and cerium [25] and coupling nitrogen containing ZnO with tungsten and vanadium oxides [26]. In this present work indium doped zinc oxide films (In-ZnO) were deposited by an atmospheric pressure aerosol assisted chemical vapour deposition (AACVD) technique, onto glass substrates from precursor suspensions containing 3 at.% indium ([In]/[Zn]) at 425 °C. We have investigated the relationship between the UV induced photocatalytic properties, resistivity, crystallinity and morphology while also briefly examining the durability of the deposited films.

2. Experimental

Film growth

Films were deposited onto glass microscope slides (VWR International, Cat. No. 631-0163) in an atmospheric pressure aerosol assisted CVD reactor, the configuration of which has been described previously [27]. All depositions were carried out at 425 °C for 20 min with a nitrogen carrier gas flow rate of 1.58 L/min. Undoped zinc oxide films were deposited from precursor solutions containing 0.1 mol/L zinc acetate ($Zn(O_2CCH_3)_2$) in methanol (MeOH). Indium doped films were deposited from 0.1 mol/L zinc acetate solutions containing a 3 at.%. suspension of indium chloride tetrahydrate ($InCl_3{\cdot}4H_2O$).

* Corresponding author. Tel.: +353 21 4904433; fax: +353 21 4904467.
E-mail address: mark.nolan@tyndall.ie (M.G. Nolan).

1010-6030/$ – see front matter © 2011 Elsevier B.V. All rights reserved.
doi:10.1016/j.jphotochem.2011.01.010

Characterisation methods

The ability of the films to degrade organic contaminants on their surface was established with a stearic acid test. The stearic acid (50 μl, 10 mmol in MeOH) was spin coated (2500 rpm, 50 s, Chemat Technology, KW-4A) onto the film surface, following a 3 h pre-activation step where the samples were left under a UV lamp. Two 18 W black light blue bulbs (BLB, 365 nm) were used as the UV light source at an intensity of 3 mW/cm^2, monitored with a UV radiometer and 365 nm sensor (UVP, UVX). The intensity was maintained by adjusting the height of the bulbs relative to the sample at the start of the experiment after a 20–30 min warm up period. Following spin coating the substrates were placed in an oven at 70 °C for 10 min before being allowed to cool to room temperature. The reduction of the CH peaks associated with the asymmetric and symmetric stretching frequencies between 2800 and 3000 cm^{-1} was monitored as a function of UV irradiation exposure (Bruker IFS 66/S FT-IR). The integrated area under the peaks (2810–2960 cm^{-1}) was then plotted against UV irradiation time and the relative rate (cm^{-1} min^{-1}) established, following a baseline correction step (concave rubber band method, 30 iterations and 100 baseline points). The morphology of the films was analysed using a Veeco D3100 atomic force microscope (AFM) operating in tapping mode with an Asylum AC160TS silicon cantilever (tetrahedral tip, radius <10 nm). X-ray diffraction was performed on a Phillips PW3719 X'pert materials research X-ray diffractometer (XRD) with a Cu K radiation source (λ = 0.154056 nm), between 2θ angles of 20° and 60°. The resistivity of the films was determined with a Keithley 617 electrometer between two coplanar aluminium contacts that had been evaporated onto the deposited films. Secondary ion mass spectroscopy (SIMS) analysis was carried out using a Cameca ims 3f using an O^{2+} primary ion bombardment and positive secondary ion detection to optimise the sensitivity to indium. The depth scales were determined by measuring the sputtered crater with a Dektak 6 M. Atomic absorption spectroscopy (SOLAAR M Series AA Spectrometer) was carried out on water samples in which an In-ZnO film and blank microscope slide were immersed for up to 3 h.

3. Results and discussion

The use of our atmospheric pressure AACVD leads to the deposition of thin films having graded uniformity characterised by the appearance of coloured fringes related to the film thickness. This is due in part to the depletion of precursors as they enter the heated reaction zone, where they undergo film growth on the substrate and reaction with the walls of the reactor. The corresponding thickness of the fringes deposited in this study was determined through FIB-SEM analysis on a ZnO film that had not been intentionally doped. As such, where relevant to the analytical technique employed, the thickness of fringe analysed is stated in the text.

SIMS analysis performed on both the undoped and In-doped samples, Fig. 1(a) and (b) respectively, confirmed there was no indium incorporated in the undoped films. Signals detected at masses 113 and 115 in the undoped trace, Fig. 1(a), which quickly decayed to zero, were attributed to molecular interferences of low mass elements appearing at the same nominal masses as the indium isotopes. Fig. 2(a) shows the X-ray diffraction data for an undoped ZnO film and (b) an In-doped ZnO film deposited from a precursor suspension containing 3 at.% indium recorded from areas of film ~215 nm thick. Studying Fig. 2(a) in more detail, it can be seen that the undoped ZnO films deposited were polycrystalline with peaks at 31.8° (2θ) (1 0 0), 34.5° (2θ) (0 0 2), 36.0° (2θ) (1 0 1), 47.4° (2θ) (1 0 2) and 56.4° (2θ) (1 1 0) with a principal (1 0 1) peak. The broad background peak between 20° and 40° (2θ) is characteristic of the glass substrate on which the films were deposited.

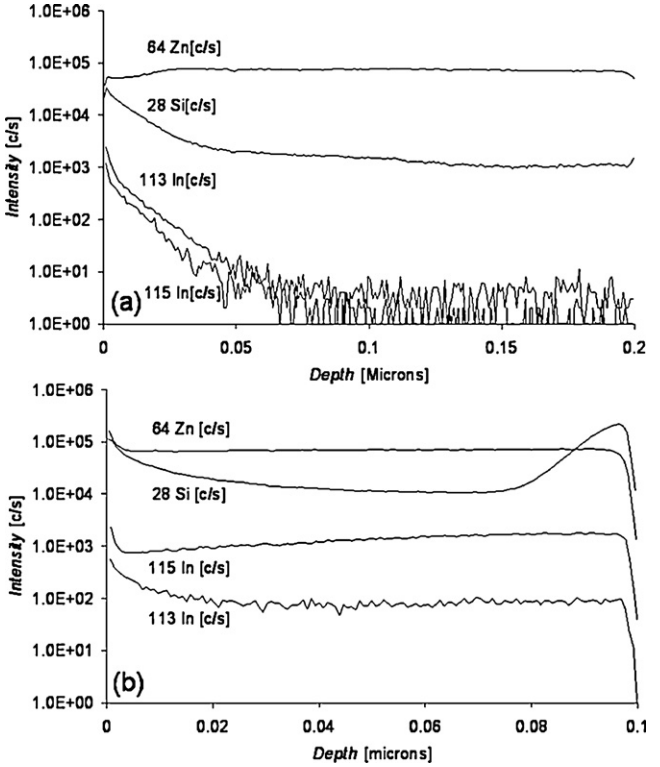

Fig. 1. (a) SIMS analysis performed on an undoped ZnO film and (b) indium doped ZnO film deposited by AACVD at 425 °C from a suspension containing 3 at.% indium.

Waugh et al. [28] investigated the effect of deposition temperature, between 400 °C and 650 °C, on the crystal orientation of ZnO films grown using AACVD from a zinc acetate precursor solution. At 400 °C their principal peak was (1 0 1) with a change towards (0 0 2) at 450 °C. In contrast Walters and Parkin [29] deposited ZnO films using AACVD from zinc acetylacetonate at 400 °C and 500 °C, reporting a dominant (0 0 2) peak at the lower deposition temperature and (1 0 0), (0 0 2), (1 0 1) and (1 0 2) planes at 500 °C. It is not clear from either study if the choice of zinc precursor directly influenced the preferred orientation of film growth. The AFM image corresponding to a representative film thickness in which the XRD was recorded for the undoped film is shown in Fig. 2(c). Spherical grain structures were observed with an average diameter of ~32 nm. The influence of introducing indium as the dopant into the ZnO films on the crystal orientation of the films is shown in Fig. 2(b). Clear evidence of a change in the preferred orientation, as defined by Conley and Ono [30] was found since a (0 0 2) peak which is at least five times higher in intensity than the (1 0 0) peak as measured by XRD, can be seen. No peaks corresponding to zinc–indium or indium oxide compounds were detected. The AFM image in Fig. 2(d) is illustrative of the surface morphology of the doped films at the film thickness the XRD was performed. Large platelet structures can clearly be seen. These were estimated to be approximately 220–230 nm in diameter. Yoshida et al. [31] deposited ZnO and In-ZnO films using spray pyrolysis with indium acetate as the dopant. Their undoped films exhibited a hexagonal wurtzite structure, while the addition of 0.5–1 at.% concentration ([In]/[Zn]) showed a striking change in preferred orientation towards the (0 0 2) plane, combined with the appearance of a morphology consisting of layered hexagonal platelets with irregular edge like grains, which decreased as the In loading reached 3 at.%. They also witnessed the preferred orientation switch to the (1 0 1) plane as the In concentration reached 7 at.%. A similar switch from (0 0 2) to (1 0 1) with In loading has been witnessed

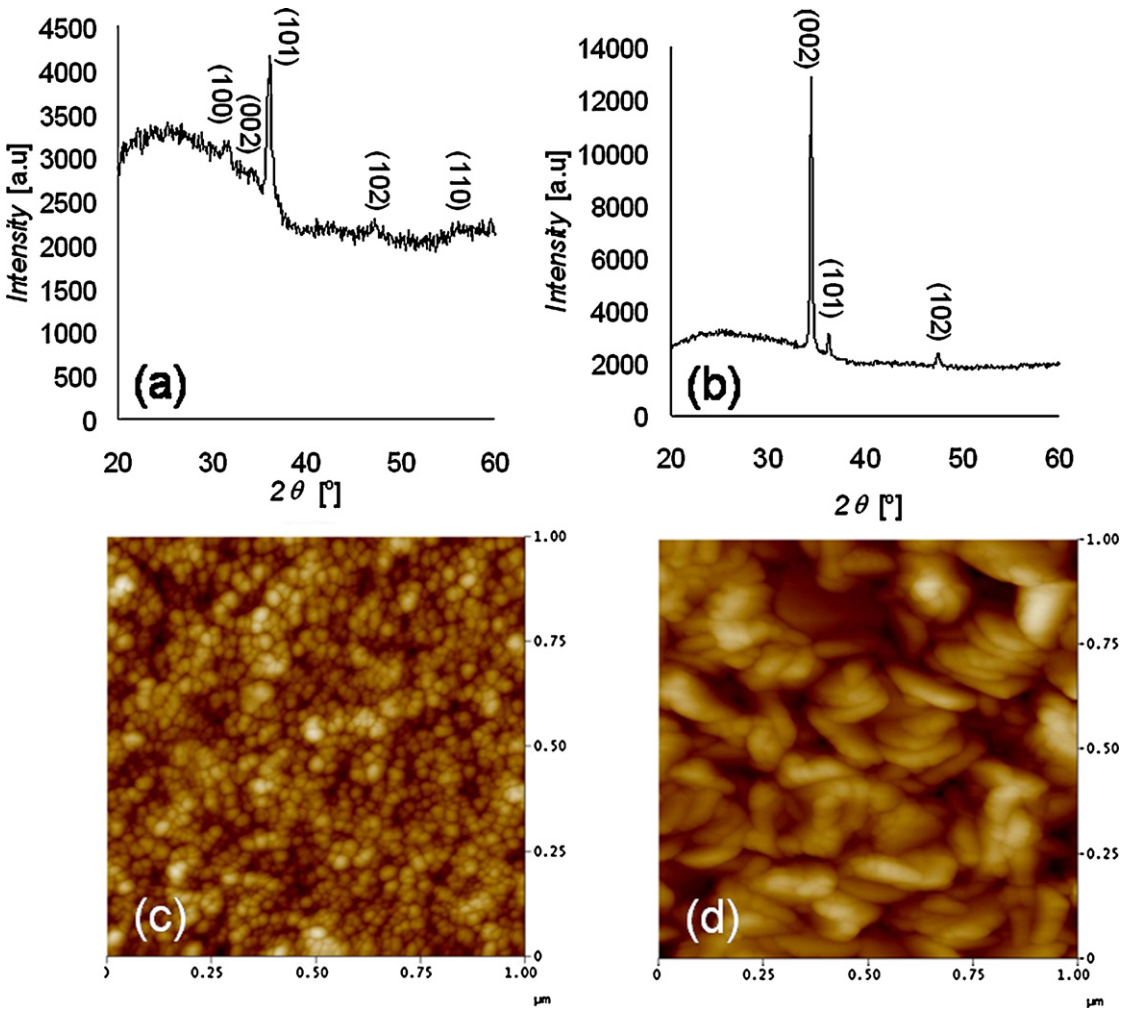

Fig. 2. (a) XRD of an undoped ZnO film, (b) XRD of an In-ZnO film deposited from a starting suspension containing 3 at.% In, (c) corresponding AFM image of the undoped ZnO film and (d) corresponding AFM image of the In-ZnO film. The XRD measurements and AFM images were taken on an area of film ~215 nm thick.

by other researchers in the area [32,33]. In contrast to the work reported by Yoshida, Lopez et al. [34] deposited In-ZnO films via a chemical spray technique using indium nitrate, sulphate, acetate and chloride as the doping sources, and found that all films exhibited a (1 0 1) preferred orientation, which was independent of the doping source and film thickness. Large flake-like structures were seen in their films deposited with indium sulphate as the doping source, whereas films deposited using indium chloride exhibited a spherical grain-like structure.

The resistivity of the undoped and In-doped films was established through the measurement of *I–V* curves, as shown in Fig. 3(a) and (b), on an area of the films ~130 nm thick. The resistance for each sample showed no significant dependence on the atmosphere in which they were measured. The sheet resistance for the undoped and In-doped films was found to be $2.21 \times 10^8\ \Omega$/sq and $5.52 \times 10^3\ \Omega$/sq corresponding to a resistivity of 2.87 kΩ cm and 0.072 Ω cm respectively, calculated from the product of the film thickness (cm) and sheet resistance (ohms). It is clear that, in addition to altering the film morphology and preferred crystal orientation, the incorporation of indium into the lattice has a significant influence on the electrical properties of the films, where the resistivity is reduced more than five orders of magnitude. A number of other researchers have seen a similar behaviour through the incorporation of indium into ZnO films. Shinde et al. [35] deposited In-doped ZnO films from aqueous zinc acetate solutions using a spray pyrolysis technique at 400 °C, followed by a 200 °C post deposition anneal. They reported a reduction in resistivity in the pre-annealed and annealed films deposited from precursor solutions containing up to 3 at.% In-doping ($InCl_3$), due to an increase in the free electron concentration following doping. Their post annealed films showed a significant increase in conductivity and mobility as compared to non-annealed samples. This was partially attributed to an improvement in the crystallinity of the films after annealing. They proposed that the enhancement of the films' crystallinity is associated with an increase in the grain size which leads to a reduction of the defects at the grain boundaries. Moreover, this reduces the scattering losses, lowering the number of electron trap states and increasing the measured carrier concentration (n). However, not all studies into the influence of In-doping on grain size report an increase in grain size. Ilican et al. [36] reported a reduction in crystallinity and grain size through the addition of In ($InCl_3$) to ZnO films deposited by spray pyrolysis. Their trend in resistivity, however, was in good agreement with Shinde et al. such that after an initial decrease in resistivity as a function of In concentration in the starting solution (1 and up to 3 at.% for Ilican and Shinde respectively), the resistivity increased. This is attributed to a reduction in the mobility through enhancement of film disorder, probably due to grain boundary segregation of In impurities, reported by Joseph et al. [37] to be $In(OH)_3$, and a subsequent dispersion of carriers. Similarly Ahmad et al. [38] prepared In-doped ZnO nanowires through thermal evaporation reporting an increase in carrier concentration and mobility leading to an increase in conductivity. It

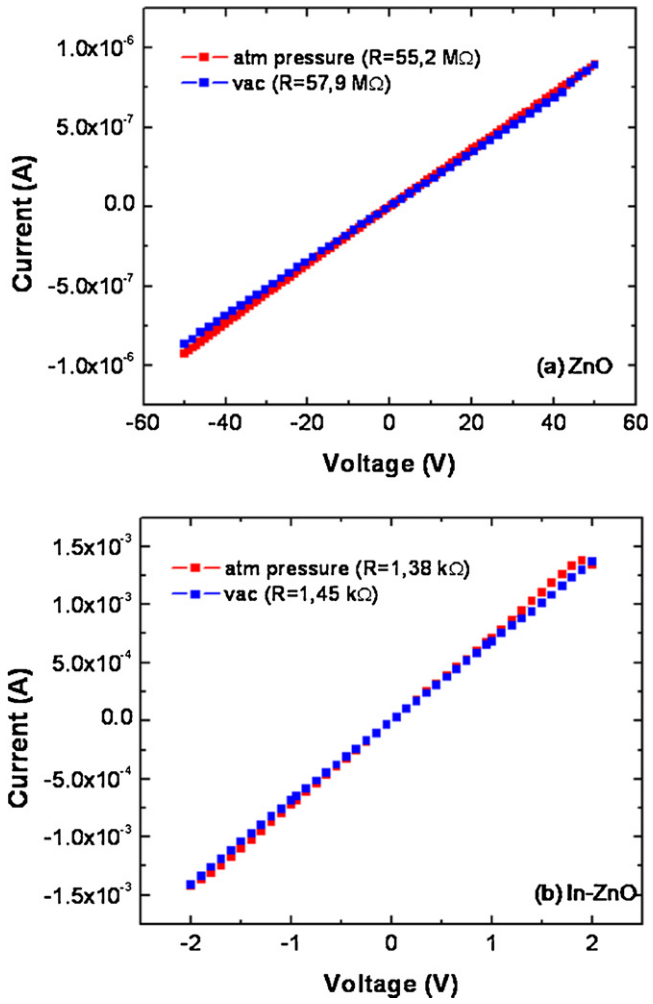

Fig. 3. (a) *I–V* curve for the undoped ZnO film and (b) for the In-ZnO film measured on an area ~130 nm thick.

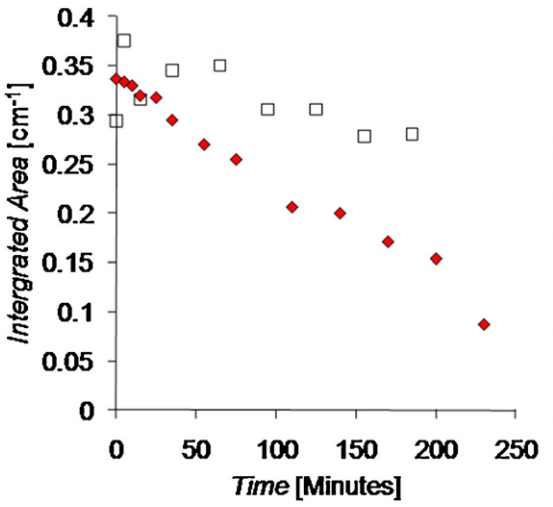

Fig. 4. Stearic acid degradation as a function of UV irradiation time for (♦) the In-ZnO doped film and (□) the undoped ZnO film.

is clear from our own study, that as well as a switch to a *c*-axis preferred orientation the crystallinity of the In-ZnO films showed a significant improvement (Fig. 2(a) and (b)), which in combination with the expected increase in carrier concentration through In-doping led to a reduction in film resistivity.

Fig. 4 shows the reduction in integrated area of the symmetric and asymmetric C–H stretching frequencies of the stearic acid molecule, recorded on the FT-IR as a function of UV irradiation time for both the In-doped and the undoped ZnO films. The mechanism through which semiconductor photocatalysts degrade organic contaminants on their surface has been previously discussed in considerable detail [39]. In short, electrons (e^-) in semiconductor photocatalysts may be promoted from the valence band to the conduction band through the absorption of a photon with energy greater or equal to the bandgap energy (E_{BG}), leaving behind a hole (h^+) in the valence band. The electron–hole pairs generated in such a way may either recombine in the bulk material, or migrate to the surface where they can undergo reduction (e^-), or oxidation (h^+), reactions with adsorbed acceptors or donors on the surface, generating photoactive species capable of decomposing organic contaminants. For example the hole may react with surface hydroxyl groups forming hydroxyl radicals that can subsequently oxidise organic contaminants. The electron may react with adsorbed oxygen to form superoxides which is reported to be reduced to hydrogen peroxide and water through intermediates that act as sources of hydroxyl radicals [40].

The stearic acid test provides a relatively simple route to evaluate the ability of photocatalytic semiconductors to oxidise surface organic contaminants under UV irradiation, and is employed by a number of research groups in the area [41–43]. Studying Fig. 4 in detail it can be seen that the In-ZnO film had a greater rate of stearic acid degradation than that of the undoped film (0.001 cm^{-1} min^{-1} compared to 0.0003 cm^{-1} min^{-1} taken from the gradient of a linear trend line plotted across the whole data set). A blank glass stearic acid test control was performed by spinning stearic acid onto a piece of blank glass substrate. The integrated area was found to be 0.00004 cm^{-1} min^{-1}. When compared to the integrated area for the doped and undoped films respectively it can be seen that the influence of the UV light on the stearic acid is minimal, and also that the rate of degradation on the undoped film is relatively low. Using a conversion factor of 9.7×10^{15} molecules of stearic acid to be equivalent to an integrated FT-IR area value of 1 cm^{-1}, as reported by Mills and Wang [44], a plot of the number of molecules of stearic acid remaining on the film, as a function of UV irradiation time was made. From the plot the initial rate of stearic acid removal (molecules per second) was calculated and used to determine the formal quantum efficiency (FQE) of the films as described by Mills and Wang using formula (1). Calculation of the FQE revealed a rate of stearic acid degradation of 1.67×10^{-6} and 5.68×10^{-6} molecules/photon for the undoped and In-doped film respectively.

$$\text{FQE (SA)} = \frac{\text{Rate of removal of SA (molecules/s)}}{\text{Rate of incident light (photons/s)}} \quad (1)$$

The samples used for the measurement had a graded film thickness due to the nature of the AACVD process as previously discussed. The maximum film thickness in each case was ~220 nm and ~150 nm for the undoped and In-doped films respectively. It would be expected that a thicker film would have a superior rate of photocatalysis due to increased light harvesting, however it can be seen in our study that the thinner In-doped film had a ~3-fold increase in the rate of stearic acid molecule removal per photon. A number of factors can influence the rate of organic degradation on the surface of semiconductor photocatalytic films, namely (1) impurities due to the film processing technique used (2) surface morphology (3) film thickness analysed (4) elemental doping and (5) crystallinity:

(1) *Impurities*: Evans et al. [45] deposited TiO_2 films by atmospheric pressure CVD on stainless steel substrates, and investigated the effectiveness of SiO_2 barrier layers, deposited by flame assisted

CVD, in preventing ions from the substrate (iron, chromium and nickel) diffusing into the TiO_2 films during the high temperature deposition process acting as recombination centres for the UV generated electron–hole pairs. Their study found that when SiO_2 barrier layers, ~30 nm and ~120 nm thick, were employed an improvement in photoactivity, determined through a stearic acid test, was seen with the thicker barrier layer proving more effective. In our particular study no barrier layers were employed to prevent diffusion of ions, particularly Na^+, from the glass substrate into the ZnO films. It is therefore conceivable that if a barrier layer were employed in future experiments, an increase in the rate at which organic contaminants are degraded may be seen. (2) *Morphology*: Ali et al. [46] investigated the relationship between film morphology and photocatalytic activity on ZnO films deposited by magnetron sputtering, hydrothermal growth and a combination of magnetron sputtered templates with a hydrothermal film overlaid. Their study found that using a sputtered template followed by hydrothermal film growth produced a well aligned rod like structure, which also possessed the greatest photoactivity during the degradation of methylene blue. In contrast films deposited hydrothermally onto plain glass substrates lacked alignment and subsequently possessed a reduced photoactivity. The AFM images shown in Fig. 2(c) and (d) clearly show a significant difference in the surface morphology of the undoped and In-doped films. In-doping produced high surface area platelet structures at film thicknesses over ~50 nm. A higher surface area can lead to a greater number of sites at which electron–hole pairs can be generated to take part in the photocatalytic reaction and helps to explain in part why, with a lower maximum film thickness in the area tested, the In-ZnO film had a higher rate of stearic acid degradation. (3) *Thickness*: Chen and Dionysiou [47] deposited dip coated layers of TiO_2 on stainless steel substrates and noted that increasing the film thickness increased the rate of photocatalytic degradation of 4-cholorobenzoic acid. This was attributed to an increase in the fraction of UV light absorbed by the film. In the case of our particular photoactivity analysis, the In-ZnO film was thinner (150 nm) than the undoped film (220 nm), eliminating this as a possible cause for the observed increase in organic degradation rate. (4) *Doping*: In terms of elemental doping of UV activated zinc oxide photocatalysts, it is commonly reported that the dopant e.g. silver, lanthanum or palladium act as traps for photogenerated electrons, reducing the incidence of electron/hole pair recombination, and increasing the number of hydroxyl radicals formed on the surface through the oxidation of surface hydroxyl groups by the hole [7–9,12,15]. (5) *Crystallinity*: Kenanakis and Katsarakis [48] investigated the degradation of stearic acid on *c*-axis orientated ZnO nanowires and saw an improved rate of photocatalytic activity for the nanowire films, as compared to the ZnO sol–gel seed layers. This was credited to their enhanced crystallinity and large surface to volume ratio. As previously discussed an improvement in crystallinity can increase grain size and reduce boundary defects and carrier scattering losses lowering the number of electron trap states which, in combination with a higher surface area for the In-ZnO film in our study, most likely accounts for the observed increase in the rate of stearic acid decomposition as compared to the thicker, undoped film.

When compared to TiO_2 thin film photocatalysts the durability of ZnO films is known to be relatively poor at extreme pH levels and under UV illumination [49]. As such we performed basic durability tests on our In-ZnO samples and found that when immersed in dilute acid (0.1 mol HCl, <5 min) and solvent (MeOH, 24 h), complete dissolution of the films occurred. Immersion of the In-ZnO film in de-ionised water appeared to have no visible effect, however atomic absorption spectroscopy measurements performed on aliquots of the deionised water, taken at 1 h intervals for up to 3 h, revealed some dissolution when compared to water samples taken from an immersed blank microscope slide (Table 1).

Table 1
Concentration of Zn found in samples of DI water in which an In-ZnO film and blank microscope slide had been immersed for up to 3 h.

	Concentration (ppb)	
	In-ZnO film	Blank Microscope Slide
DI water	22.0	0
1 h	124.7	16.1
2 h	191.3	17.9
3 h	156.5	16.7

Liang and Weimer [50] have recently published data on the photoactivity passivation of titanium dioxide nanoparticles by molecular layer deposition (MLD) of alucone and atomic layer deposition (ALD) of aluminium oxide (Al_2O_3) showing the particles retained a significant amount of photoactivity when coated with a ~1.2 nm thick Al_2O_3 film which then decayed to zero as a ~3.6 nm film was overlaid. The ALD technique is well known for depositing thin films that have excellent uniformity and conformallity, and Al_2O_3 is recognised as an electrical insulator with excellent chemical resistance in acidic and basic conditions. What is interesting to note is that despite the insulating properties of Al_2O_3 it is still possible for the electron–hole pairs to migrate through the TiO_2 and thin Al_2O_3 film to take part in photocatalytic reduction and oxidation reactions on the surface. It may be possible with careful film selection and process conditions to overlay a protective film that would improve the durability of the ZnO, while retaining sufficient photocatalytic activity on the protective films surface.

4. Conclusions

We have grown undoped and In-doped ZnO films on glass substrates using an atmospheric pressure chemical vapour deposition technique. We have shown that In-ZnO deposited in this way exhibits UV induced photocatalytic properties, combined with a decrease in resistivity as compared to undoped films. Adding indium to the zinc oxide precursor solution influenced the preferred orientation and morphology of film growth with the *c*-axis plane becoming dominant, while also producing a surface characterised by large platelet structures. The combination of morphology and crystallinity is believed to account for the observed improvement in the rate of organic contaminant decomposition when compared to the undoped films, most likely due to a reduction in the recombination rate of the electron–hole pairs at grain boundaries, and a larger surface area on which photocatalytic species (hydroxyl radicals and superoxides) may form. However the durability of the films during simple tests proved to be quite poor. As such practical applications involving a combination of the visible light transparency, the conductivity and the self-cleaning abilities of the In-ZnO films are limited in their current state. We propose that it may be possible to improve the durability of the In-ZnO films through the deposition of a suitable thin film that allows the underlying In-ZnO to retain its photocatalytic and conductive properties. Atomic layer deposition, with its ability to conformally coat complex structures would be a suitable technique for this.

Acknowledgements

The authors would like to acknowledge the financial support of Science Foundation Ireland (SFI, Principal Investigator research grant 07/IN.1/I787). The authors would also like to thank Michael Schimdt, Tyndall National Institute, for the FIB-SEM analysis, Loughborough Scientific for ToF-SIMS analysis and John Meehan, University College Cork, for the atomic absorption spectroscopy.

References

[1] S.S. Badadhe, I.S. Mulla, H_2S gas sensitive indium-doped ZnO thin films: preparation and characterization, Sensors and Actuators B 143 (2009) 164–170.
[2] G. Bernardo, G. Goncalves, P. Barquinha, Q. Ferreira, G. Brotas, L. Pereira, A. Charas, J. Morgado, R. Martins, E. Fortunato, Polymer light-emitting diodes with amorphous indium–zinc oxide anodes deposited at room temperature, Synthetic Metals 159 (2009) 1112–1115.
[3] K.-M. Uang, S.-J. Wang, S.-L. Chen, T.-M. Chen, B.-W. Liou, The use of transparent indium–zinc oxide/(oxidized-Ni/Au) ohmic contact to GaN-based light-emitting diodes for light output improvement, Thin Solid Films 515 (4) (2006) 2501–2506.
[4] S. Major, K.L. Chopra, Indium-doped zinc oxide films as transparent electrodes for solar cells, Solar Energy Materials 17 (5) (1988) 319–327.
[5] E. Fortunato, P. Barquinha, G. Goncalves, L. Pereira, R. Martins, High mobility and low threshold voltage transparent thin film transistors based on amorphous indium zinc oxide semiconductors, Solid State Electronics 52 (3) (2008) 443–448.
[6] Z. Yanning, T. Honghui, C. Limin, W. Fuji, Studies on the bactericidal performance of indium doped nano-zinc oxide, Huazhong Shifan Daxue Xuebao (Ziran Kexue Ban) 42 (2008) 400.
[7] R. Georgekutty, M.K. Seery, S.C. Pillai, A highly efficient Ag–ZnO photocatalyst: synthesis, properties, and mechanism, Journal of Physical Chemistry C 112 (35) (2008) 13563–13570.
[8] C.A.K. Gouvea, F. Wypych, S.G. Moraes, N. Duran, P.P. Zamora, Semiconductor-assisted photodegradation of lignin, dye, and kraft effluent by Ag-doped ZnO, Chemosphere 40 (4) (2000) 427–432.
[9] M.J. Height, S.E. Pratsinis, O. Mekasuwandumrong, P. Praserthdam, Ag–ZnO catalysts for UV-photodegradation of methylene blue, Applied Catalysis B: Environmental 63 (3–4) (2006) 305–312.
[10] M.A. Behnajady, N. Modirshahla, M. Shokri, A. Zeininezhad, H.A. Zamani, Enhancement photocatalytic activity of ZnO nanoparticles by silver doping with optimization of photodeposition method parameters, Journal of Environmental Science and Health Part A 44 (7) (2009) 666–672.
[11] T. Jia, W. Wang, F. Long, Z. Fu, H. Wang, Q. Zhang, Fabrication, characterization and photocatalytic activity of La-doped ZnO nanowires, Journal of Alloys and Compounds 484 (1–2) (2009) 410–415.
[12] S. Anandan, A. Vinu, K.L.P. Sheeja Lovely, N. Gokulakrishnan, P. Srinivasu, T. Mori, V. Murugesan, V. Sivamurugan, K. Ariga, Photocatalytic activity of La-doped ZnO for the degradation of monocrotophos in aqueous suspension, Journal of Molecular Catalysis A: Chemical 266 (1–2) (2007) 149–157.
[13] S. Anandan, A. Vinu, T. Mori, N. Gokulakrishnan, P. Srinivasu, V. Murugesan, K. Ariga, Photocatalytic degradation of 2,4,6-trichlorophenol using lanthanum doped ZnO in aqueous suspension, Catalysis Communications 8 (9) (2007) 1377–1382.
[14] K.-C. Hsiao, S.-C. Liao, Y.-J. Chen, Synthesis, characterization and photocatalytic property of nanostructured Al-doped ZnO powders prepared by spray pyrolysis, Materials Science and Engineering A 447 (1–2) (2007) 71–76.
[15] Y. Chang, J. Xu, Y. Zhang, S. Ma, L. Xin, L. Zhu, C. Xu, Optical properties and photocatalytic performances of Pd modified ZnO samples, Journal of Physical Chemistry C 113 (43) (2009) 18761–18767.
[16] X. Qiu, L. Li, J. Zheng, J. Liu, X. Sun, G. Li, Origin of the enhanced photocatalytic activities of semiconductors: a case study of ZnO doped with Mg^{2+}, Journal of Physical Chemistry C 112 (32) (2008) 12242–12248.
[17] D. Li, H. Haneda, Synthesis of nitrogen-containing ZnO powders by spray pyrolysis and their visible-light photocatalysis in gas-phase acetaldehyde decomposition, Journal of Photochemistry and Photobiology A: Chemistry 155 (1–3) (2003) 171–178.
[18] J. Lu, Q. Zhang, J. Wang, F. Saito, M. Uchida, Synthesis of N-Doped ZnO by grinding and subsequent heating ZnO–urea mixture, Powder Technology 162 (1) (2006) 33–37.
[19] C. Shifu, Z. Wei, Z. Sujuan, L. Wei, Preparation, characterization and photocatalytic activity of N-containing ZnO powder, Chemical Engineering Journal 148 (2–3) (2009) 263–269.
[20] K.G. Kanade, B.B. Kale, J.-O. Baeg, S.M. Lee, C.W. Lee, S.-J. Moon, H. Chang, Self-assembled aligned Cu doped ZnO nanoparticles for photocatalytic hydrogen production under visible light irradiation, Materials Chemistry and Physics 102 (1) (2007) 98–104.
[21] J.-Z. Kong, A.-D. Li, H.-F. Zhai, Y.-P. Gong, H. Li, D. Wu, Preparation, characterization of the Ta-doped ZnO nanoparticles and their photocatalytic activity under visible-light illumination, Journal of Solid State Chemistry 182 (8) (2009) 182, 2061-2067.
[22] L. Li, W. Wang, H. Liu, X. Liu, Q. Song, S. Ren, First principles calculations of electronic band structure and optical properties of Cr-doped ZnO, Journal of Physical Chemistry C 113 (19) (2009) 8460–8464.
[23] R. Ullah, J. Dutta, Photocatalytic degradation of organic dyes with manganese-doped ZnO nanoparticles, Journal of Hazardous Materials 156 (1–3) (2008) 194–200.
[24] L. -Chuan Chen, Y.-J. Tu, Y.-S. Wang, R.-S. Kan, C.-M. Huang, Characterization and photoreactivity of N-, S-, and C-doped ZnO under UV and visible light illumination, Journal of Photochemistry and Photobiology A: Chemistry 100 (2–3) (2008) 170–178.
[25] J. Iqbal, X. Liu, H. Zhu, Z.B. Wu, Y. Zhang, D. Yu, R. Yu, Raman and highly ultraviolet red-shifted near band-edge properties of LaCe-co-doped ZnO nanoparticles, Acta Materialia 57 (16) (2009) 4790–4796.
[26] D. Li, H. Haneda, Enhancement of photocatalytic activity of sprayed nitrogen-containing ZnO powders by coupling with metal oxides during the acetaldehyde decomposition, Chemosphere 54 (8) (2004) 1099–1110.
[27] S. O'Brien, M.G. Nolan, M. Çopuroglu, J.A. Hamilton, I. Povey, l. Pereira, R. Martins, E. Fortunato, M. Pemble, Zinc oxide thin films: characterization and potential applications, Thin Solid Films 518 (16) (2010) 4515–4519.
[28] M.R. Waugh, G. Hyett, I.P. Parkin, Zinc oxide thin films grown by aerosol assisted CVD, Chemical Vapor Deposition 14 (11–12) (2008) 366–372.
[29] G. Walters, I.P. Parkin, Aerosol assisted chemical vapour deposition of ZnO films on glass with noble metal and p-type dopants; use of dopants to influence preferred orientation, Applied Surface Science 255 (13–14) (2009) 6555–6560.
[30] J.F. Conley, Y. Ono, United States Patent US 7597757 B2 (2009).
[31] M. Miki-Yoshida, F. Paraguay-Delgado, W. Estrada-Lopez, E. Andrade, Structure and morphology of high quality indium-doped ZnO films obtained by spray pyrolysis, Thin Solid Films 376 (1–2) (2000) 99–109.
[32] M. Krunks, E. Mellikov, Zinc oxide thin films by the spray pyrolysis method, Thin Solid Films 270 (1–2) (1995) 33–36.
[33] F. Paraguay-Delgado, J. Morales, W. Estrada-Lopez, E. Andrade, M. Miki-Yoshida, Influence of Al, In, Cu, Fe and Sn dopants in the microstructure of zinc oxide thin films obtained by spray pyrolysis, Thin Solid Films 366 (1–2) (2000) 16–27.
[34] M.A. Lucio-Lopez, A. Maldonado, R. Castanedo-Perez, G. Torres-Delgado, M. de la, L. Olvera, Thickness dependence of ZnO: in thin films doped with different indium compounds and deposited by chemical spray, Solar Energy Materials and Solar Cells 90 (15) (2006) 2362–2376.
[35] S.S. Shinde, P.S. Shinde, C.H. Bhosale, K.Y. Rajpure, Optoelectronic properties of sprayed transparent and conducting indium doped zinc oxide thin films, Journal of Physics D: Applied Physics 41 (10) (2008) 105109–105115.
[36] S. Ilican, Y. Caglar, M. Caglar, B. Demirci, Polycrystalline indium-doped ZnO thin films: preparation and characterization, Journal of Optoelectronics and Advanced Materials 10 (10) (2008) 2592–2598.
[37] B. Joseph, P.K. Manoj, V.K. Vaidyan, Studies on preparation and characterization of indium doped zinc oxide films by chemical spray deposition, Bulletin of Materials Science 28 (5) (2005) 487–493.
[38] M. Ahmad, J. Zhao, J. Iqbal, W. Miao, L. Xie, R. Mo, J. Zhu, Conductivity enhancement by slight indium doping in ZnO nanowires for optoelectronic applications, Journal of Physics D: Applied Physics 42 (16) (2009) 165406–165413.
[39] A. Mills, S.-K. Lee, A web-based overview of semiconductor photochemistry-based current commercial applications, Journal of Photochemistry and Photobiology A: Chemistry 152 (1–3) (2002) 233–247.
[40] A. Mills, S. Hodgen, S.-K. Lee, Self-cleaning titania films: an overview of direct, lateral and remote photo-oxidation processes, Research on Chemical Intermediates 31 (4–6) (2005) 295–308.
[41] A. Mills, M. McFarlane, Current and possible future methods of assessing the activities of photocatalyst films, Catalysis Today 129 (1–2) (2007) 22–28.
[42] P. Evans, S. Mantke, A. Mills, A. Robinson, D.W. Sheel, A comparative study of three techniques for determining photocatalytic activity, Journal of Photochemistry and Photobiology A: Chemistry 188 (2–3) (2007) 387–391.
[43] S. O'Neill, I.P. Parkin, R.J.H. Clark, A. Mills, N. Elliot, Photocatalytically active γ-WO_3 films from atmospheric pressure CVD of $WOCl_4$ with ethyl acetate or ethanol, Chemical Vapor Deposition 10 (3) (2004) 136–141.
[44] A. Mills, J. Wang, Simultaneous monitoring of the destruction of stearic acid and generation of carbon dioxide by self-cleaning semiconductor photocatalytic films, Journal of Photochemistry and Photobiology A: Chemistry 182 (2006) 181–186.
[45] P. Evans, T. English, D. Hammond, M.E. Pemble, D.W. Sheel, The role of SiO_2 barrier layers in determining the structure and photocatalytic activity of TiO_2 films deposited on stainless steel, Applied Catalysis A: General 321 (2) (2007) 140–146.
[46] A.M. Ali, E.A.C. Emanuelsson, D.A. Patterson, Photocatalysis with nanostructured zinc oxide thin films: the relationship between morphology and photocatalytic activity under oxygen limited and oxygen rich conditions and evidence for a Mars Van Krevelen mechanism, Applied Catalysis B: Environmental 97 (1–2) (2010) 168–181.
[47] Y. Chen, D.D. Dionysiou, Correlation of structural properties and film thickness to photocatalytic activity of thick TiO_2 films coated on stainless steel, Applied Catalysis B: Environmental 69 (1–2) (2006) 24–33.
[48] G. Kenanakis, N. Katsarakis, Light-induced photocatalytic degradation of stearic acid by *c*-axis oriented ZnO nanowires, Applied Catalysis A: General 378 (2) (2010) 227–233.
[49] J. Han, W. Qiu, W. Gao, Potential dissolution and photo-dissolution of ZnO thin films, Journal of Hazardous Materials 178 (1–3) (2010) 115–122.
[50] X. Liang, A.W. Weimer, Photoactivity passivation of TiO_2 nanoparticles using molecular layer deposited (MLD) polymer films, Journal of Nanoparticle Research 12 (1) (2010) 135–142.